Finite element method for calculating spectral and optical characteristics of axially symmetric quantum dots

A. A. Gusev, O. Chuluunbaatar, S. I. Vinitsky, V. L. Derbov, L. L. Hai, et al.

A. A. Gusev, O. Chuluunbaatar, S. I. Vinitsky, V. L. Derbov, L. L. Hai, E. M. Kazaryan, H. A. Sarkisyan, "Finite element method for calculating spectral and optical characteristics of axially symmetric quantum dots," Proc. SPIE 10717, Saratov Fall Meeting 2017: Laser Physics and Photonics XVIII; and Computational Biophysics and Analysis of Biomedical Data IV, 1071712 (26 April 2018); doi: 10.1117/12.2315720

SPIE.

Event: Saratov Fall Meeting 2017, 2017, Saratov, Russian Federation

Finite element method for calculating spectral and optical characteristics of axially symmetric quantum dots

A.A. Gusev[a], O. Chuluunbaatar[a,b], S.I. Vinitsky[a,c], V.L. Derbov[d], L.L. Hai[e], E. M. Kazaryan[f], and H. A. Sarkisyan[f,g]

[a] Joint Institute for Nuclear Research, Dubna, Russia
[b] Institute of Mathematics, National University of Mongolia, Ulaanbaatar, Mongolia
[c]RUDN University, Moscow, Russia, 6 Miklukho-Maklaya st, Moscow, 117198
[d]N.G. Chernyshevsky Saratov National Research State University, Saratov, Russia
[e] Ho Chi Minh city University of Education, Ho Chi Minh city, Vietnam
[f]Russian-Armenian (Slavonic) University, H. Emin 123, 0051 Yerevan, Armenia
[g]Peter the Great Saint-Petersburg Polytechnic University, Polytechnicheskaya 29, St. Petersburg 195251, Russia

ABSTRACT

We present new calculation schemes using high-order finite element method implemented on unstructured grids with triangle elements for solving boundary-value problems that describe axially symmetric quantum dots. The efficiency of the algorithms and software is demonstrated by benchmark calculations of the energy spectrum, the envelope eigenfunctions of electron, hole and exciton states, and the direct interband light absorption in conical and spheroidal impenetrable quantum dots.
Key words: conical and spheroidal quantum dots, energy spectra, light absorption, finite element method

1. INTRODUCTION

The study of spectral and optical characteristics of quantum dots (QDs) with complicated geometry is an actual problem of both computational and theoretical physics. To solve the boundary-value problems (BPVs) that describe the models of QDs, they commonly use finite-difference and variational methods,[1] finite element method (FEM),[2] Kantorovich and adiabatic methods.[3,4]

In this paper, we consider new high-order FEM calculation schemes[5,6] implemented on unstructured grids with triangle elements for solving the BVPs that describe axially symmetric QDs, in comparison with Kantorovich method (KM) and adiabatic approach (AA). We discuss the application of these methods and the appropriate software to the calculation of the energy spectra of electron, hole and exciton states in axially symmetric QDs, the direct interband light absorption and the light absorption coefficient (AC) in ensembles of non-interacting QDs by the example of conical and spheroidal impenetrable QDs.

2. SETTING THE PROBLEM

Within the effective mass approximation we consider a class of QD models in which the calculation of energy levels and the corresponding envelope eigenfunctions is reduced to self-adjoint BVPs for elliptic differential equations[7]

$$(D-E)\,\Psi(z) \equiv \left(-\frac{1}{g_0(z)} \sum_{ij=1}^{d} \frac{\partial}{\partial z_i} g_{ij}(z) \frac{\partial}{\partial z_j} + V(z) - \mathcal{E} \right) \Psi(z) = 0. \tag{1}$$

We assume that $g_0(z) > 0$, $g_{ji}(z) = g_{ij}(z)$ and $V(z)$ are real-valued functions, continuous together with their generalized derivatives to a given order in the domain $z \in \bar{\Omega} = \Omega \cup \partial\Omega$ with the piecewise continuous boundary

Send correspondence to V.L.D.: E-mail: derbovvl@gmail.com, Telephone: +7 927 220 8353

Saratov Fall Meeting 2017: Laser Physics and Photonics XVIII; and Computational Biophysics and Analysis of Biomedical Data IV, edited by Vladimir L. Derbov, Dmitry E. Postnov, Proc. of SPIE Vol. 10717, 1071712 · © 2018 SPIE · CCC code: 1605-7422/18/$18 · doi: 10.1117/12.2315720

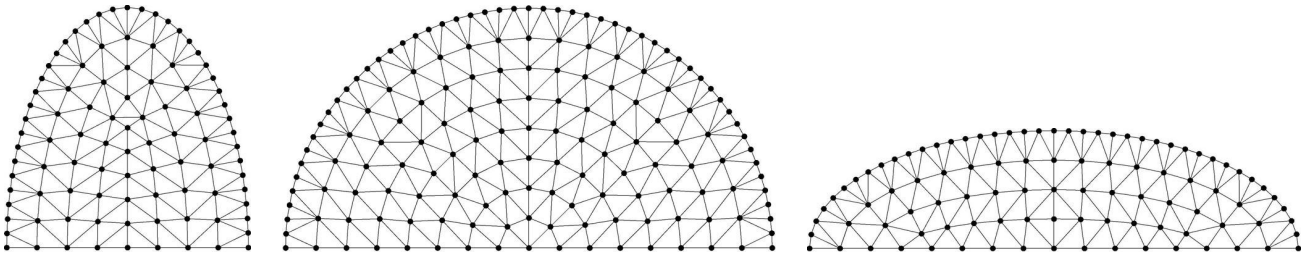

Figure 1. Triangle grid in the form of a polygon with $n = 52$ edges for the unit sphere $R_1 = 1$ (middle panel), the oblate spheroid ($a = 1$, $c = 0.5$, left-hand panel), and the prolate one ($a = 0.5$, $c = 1$, right-hand panel), $\rho^2/a^2 + z^2/c^2 = 1$. The coordinates z and ρ are the abscissa and the ordinate, respectively.

$S = \partial\Omega$, which provides the existence of a nontrivial solutions obeying the mixed boundary conditions (BCs) of the first (I) and/or the second kind (II), i.e., Dirichlet and/or Neumann conditions

$$(I)\Psi(z)|_S = 0, \quad (II)\frac{\partial\Phi(z)}{\partial n_D}\Big|_S = 0, \quad \frac{\partial\Psi(z)}{\partial n_D} = \sum_{ij=1}^{d}(\hat{n},\hat{e}_i)g_{ij}(z)\frac{\partial\Psi(z)}{\partial z_j}, \tag{2}$$

where $\frac{\partial\Psi_m(z)}{\partial n_D}$ is the derivative along the conormal direction, $\hat{n}$ is the outer normal to the boundary of the domain $S = \partial\Omega$, $\hat{e}_i$ is the unit vector of $z = \sum_{i=1}^{d}\hat{e}_i z_i$, and $(\hat{n},\hat{e}_i)$ is the scalar product in $\mathcal{R}^d$. The eigenfunctions $\Phi_m(z)$ from the Sobolev space $H_2^{s\geq 1}(\Omega)$, $\Psi_m(z) \in H_2^{s\geq 1}(\Omega)$, corresponding to the real eigenvalues of energy spectrum $\mathcal{E}$: $\mathcal{E}_1 \leq \mathcal{E}_2 \leq ... \leq \mathcal{E}_t \leq ...$ satisfy the normalization and orthogonality conditions

$$\langle\Psi_t(z)|\Psi_{t'}(z)\rangle = \int_\Omega dz g_0(z)\Psi_t(z)\Psi_{t'}(z) = \delta_{tt'}, \quad dz = dz_1...dz_d. \tag{3}$$

We solve this problem using high-accuracy finite element schemes, implemented in the appropriate algorithms and programs.[5,6]

3. NUMERICAL CALCULATIONS OF THE ENERGY SPECTRUM

After the separation of the angular variable φ, the axially symmetric BVP for the electron, hole, and exciton eigenstates in an unpenetrable conical quantum dot (CQD) or spheroidal quantum dot (SQD) is reduced to the BVP (1)–(3) with respect to the radial $z_1 = \rho$ and the axial $z_2 = z$ variables, where $g_0(z) = \rho, g_{11}(z) = g_{22}(z) = \rho, g_{12}(z) = 0$, $V(\rho,z) = \frac{m^2}{\rho^2} + 2V_C(\rho,z)$, and $d = 2$ with the mixed conditions at the boundary $\partial\Omega = \partial\Omega_1 \cup \partial\Omega_2$, $\partial\Omega_1 = \{(\rho,z)|z = 0, \rho = \rho_{\max}(z)\}$, $\partial\Omega_2 = \{(\rho,z)|\rho = 0\}$ of the 2D domain $\Omega = \{(\rho,z)|\rho \geq 0, z \geq 0, \rho \leq \rho_{\max}(z)\}$

$$\Psi(\rho,z)|\partial\Omega_2 = 0, \quad \lim_{\rho\to 0}\left(\rho\frac{\Psi(\rho,z)}{\partial\rho}\delta_{m0} + \Psi(\rho,z)(1-\delta_{m0})\right)\Big|\,\partial\Omega_1 = 0.$$

Below we restrict ourselves to the case $m = 0$. For CDQ $\rho_{\max}(z) = R(1 - z/H)$, where R is the base radius and H is the height, while for SDQ, $\rho^2/a^2 + z^2/c^2 = 1$, $\rho^2 = x^2/a^2 + y^2/a^2$ where a and c are the spheroid semiaxes, and $\rho_{\max}(z) = a\sqrt{1 - z^2/c^2}$. Figure 1 presents a triangle finite element grid covering the domain Ω for SDQ.

For oblate and prolate SDQs the BVP (1)– (3) was also solved in the spheroidal coordinates ($z_1 = \xi, z_2 = \eta$), $g_0 = (f/2)^2(\xi^2 \pm \eta^2)$, $g_{11} = (\xi^2 \pm 1)$, $g_{22} = (1 - \eta^2)$ $(f/2)^2 = \pm(a^2 - c^2)$, f is a focal distance, and using the Kantorovich method with 60 basis functions. The comparison of results obtained for eigenvalues of oblate SDQ in the cylindrical coordinates on different FEM grids (see Figure 1), in the spheroidal coordinates, and using the (KM) is resented in Table 1*. As seen from Table 1, the results coincide to five significant digits, and the maximal contribution to the error in cylindrical coordinates is due to the error of approximating the curved boundary by triangle finite elements with rectilinear boundaries.

*For electron(e) and hole(h) states $2V_C(\rho,z) = 0$, and for exciton states $2V_C(\rho,z) = -2/\sqrt{\rho^2 + z^2}$, $2V_C(\rho,z) = \tilde{V}_C(\tilde{\rho},\tilde{z})/E_R$, $\tilde{V}_C(\tilde{\rho},\tilde{z}) = -2e/(\kappa\sqrt{\tilde{\rho}^2 + \tilde{z}^2})$, where e and m_e are the electron charge and mass, κ is the static permittivity. For GaAs model we use the reduced atomic units, $m_e^* = 0.067m_e$, $m_h^* = m_e^*/0.12$, $\kappa = 13.18$, $a_B = 104$Å, $E_R = 5.275$ meV, i.e., $\mathcal{E} = 2E = \tilde{E}/E_R$, $\Psi(\rho,z) = a_B^{3/2}\tilde{\Psi}^e(\tilde{\rho},\tilde{z})$, $\rho = \tilde{\rho}/a_B$, $z = \tilde{z}/a_B$, where $\tilde{E}$, $\tilde{V}_C(\tilde{\rho},\tilde{z})$, $\tilde{\rho}$ and $\tilde{z}$ are dimensioned quantities.

Table 1. The first three eigenvalues, $\mathcal{E}_t(n_b, l_{\min})$ in the units of E_R, for the oblate SQD $a = 2.5$, $c = 0.5$ obtained on the different FEM grid with the maximal element size $l_{\min}$. The number n_b determines the length of the polygonal boundary approximating the boundary of SQD. KM - Kantorovich method with 60 basis functions from.[3] SPH - FEM in spheroidal coordinates on non-uniform grid in the rectangular domain $0 < \xi_0 < c/\sqrt{a^2 - c^2} = 1/2\sqrt{6}$, $0 \le \eta \le 1$.

$l_{\min}$	0.0625	0.125	0.03125	0.0625	KM	SPH
n_b	0.03125	0.03125	0.015625	0.015625		
1	12.76518	12.76516	12.76490	12.76490	12.764809	12.77105
2	20.04147	20.04143	20.04086	20.04085	20.040651	20.04933
3	29.74910	29.74902	29.74780	29.74779	29.747387	29.75713

4. ADIABATIC APPROXIMATION

For classification and approximate calculation of the spectrum under the size quantization conditions for electron (e) hole (h) states the AA is used, $\Psi(x_f, x_s) = \Phi(x_f; x_s)\chi(x_s)$. For prolate SQD $a/c \ll 1$ and CQD with small apex angle $R/H \ll 1$, the parametric spectrum and eigenfunctions $\Phi(\rho; z)$ at $x_f = \rho, x_s = z$ of the "fast" subsystem at each value of parameter z are expressed in terms of the cylindrical Bessel function of the first kind[3,4]

$$2E_{n_{\rho p}m}(z) = \frac{\alpha^2_{n_{\rho p}+1,|m|}}{\rho_{\max}(z)^2}, \quad \Phi_{n_{\rho p}m}(\rho; z) = \frac{\sqrt{2}J_{|m|}(\rho\sqrt{2E_i(z)})}{\rho_{\max}(z)J_{|m+1|}(\alpha_{n_{\rho p}+1,|m|})},$$

where $\alpha_{n_{\rho p}+1,|m|}$ is the $n_p = n_{\rho p}+1$-th positive zero of the Bessel function[8] $J_{|m|}(\rho_{\max}(z))$, $n_p = n_{\rho p}+1 = 1, 2, ...$ The spectrum and eigenfunctions $\chi(z)$ of the"slow" subsystem are solutions of the BVP

$$(-\frac{\partial^2}{\partial z^2} + 2E_{n_{\rho p}}(z) - 2E_{n_{\rho p}n_{zp}})\chi_{n_{zp}n_{\rho p}}(z) = 0, \quad \int_\Omega dz\chi_{n_{zp}n_{\rho p}}(z)\chi_{n'_{zp}n_{\rho p}}(z) = \delta_{n_{zp}n'_{zp}} \tag{4}$$

with the BCs $\chi_{n_{zp}n_p}(0)$=$\chi_{n_{zp}n_p}(H)$=0 or $\chi_{n_{zp}n_p}(-c)$=$\chi_{n_{zp}n_p}(c)$=0. Considering (4) in the linear or quadratic approximation for the prolate CQD or SQD leads to the spectrum and eigenfunctions in the analytical form [3,4]

$$\mathcal{E}^{CQD}_{(tn_pn_{zp}m)}=2E^{(0)}_{n_pm} + 2\varepsilon_{n_{zp}}=\frac{2\alpha^2_{n_p,|m|}}{R^2}-\left(\frac{2\alpha^2_{n_p,|m|}}{R^2H}\right)^{2/3}\beta_{n_{zp}+1}, \quad \mathcal{E}^{PSQD}_{(tn_pn_{zp}m)}=\frac{\alpha^2_{n_p,|m|}}{a^2}+\frac{\alpha^2_{n_p,|m|}}{ac}(2n_{zp}+1),$$

where $\beta_{n_{zp}+1}$ is the i-th negative zero of the Airy function of the first kind.[8] For oblate SQD $c/a \ll 1$ and CQD $H/R \ll 1$, using the AA at $x_f = z, x_s = \rho$, one has the spectrum and eigenfunctions classified by set $[n_{zo}, n_{\rho o}]$.

Table 2 presents the comparison of the energy of Coulomb interaction of exciton $\mathcal{E}^{eh}_t = \mathcal{E}^C_t m^*_h/(m^*_e+m^*_h) - \mathcal{E}^{SQ}_t$ with the size quantization electron energy $\mathcal{E}^{SQ}_t$ at different geometric parameters of a CQD, where exciton energy $\mathcal{E}^C_t$ with the electron-hole reduced mass $m_{eh} = m^*_e m^*_h/(m^*_e + m^*_h)$ in the exciton center-of-mass frame and size quantization electron energy $\mathcal{E}^{SQ}_t$ with the electron mass m^*_e were obtained by solving the BVP(1)–(3) with Coulomb potential $2V_C(\rho, z)$ and without it, correspondingly. From Table 2 the correction energy $\mathcal{E}^{eh}_t$ is always seen to be negative, and with the increasing radius R the relative contribution of Coulomb energy of exciton becomes significant. The comparison with $\mathcal{E}^{SQ}_{(tn_pn_{zp}m)}$ and $\mathcal{E}^{eh}_{(tn_pn_{zp}m)}$ calculated using the AA and the first-order perturbation theory[4] show the contribution of nonadiabatic corrections and the applicability of the AA.

Figures 2 a and 2 b for CQD and SQD show the dependence of the charge carrier energies upon the base radius of fixed-height CQDs and upon the apex angle of fixed-volume CQDs, respectively. Note that each eigenlevel of the "fast" subsystem has a family of "slow" subsystem eigenlevels positioned thereupon. For example, for CQD with $\tilde{R} = 0.5a_B$, $\tilde{H} = 10a_B$, the first level ($(t, n_\rho, n_z) = (1, 0, 0)$, $\tilde{E}^{SQ}_1/E_R = 30.42114$) and the eighteenth ($(t, n_\rho, n_z) = (18, 1, 0)$, $\tilde{E}^{SQ}_{18}/E_R = 142.96526$) one belong to the "fast" subsystem levels. For $\tilde{R} = 1.5a_B$ the first level and the seventh one belong to the "fast" subsystem, while five levels between them belong to the "slow" subsystem, etc. The carrier energy is seen to decrease with the increasing base radius $\tilde{R}$ or small semiaxis $\tilde{a}$, because the size quantization contribution to the energy decreases. The crossing of the seventh level with the eighth one at $\tilde{R} \approx 1.5a_B$ in Fig.2a corresponds to the crossing of the same levels at $\theta_0 \approx \arctan(3/20)$ in Fig.3a.

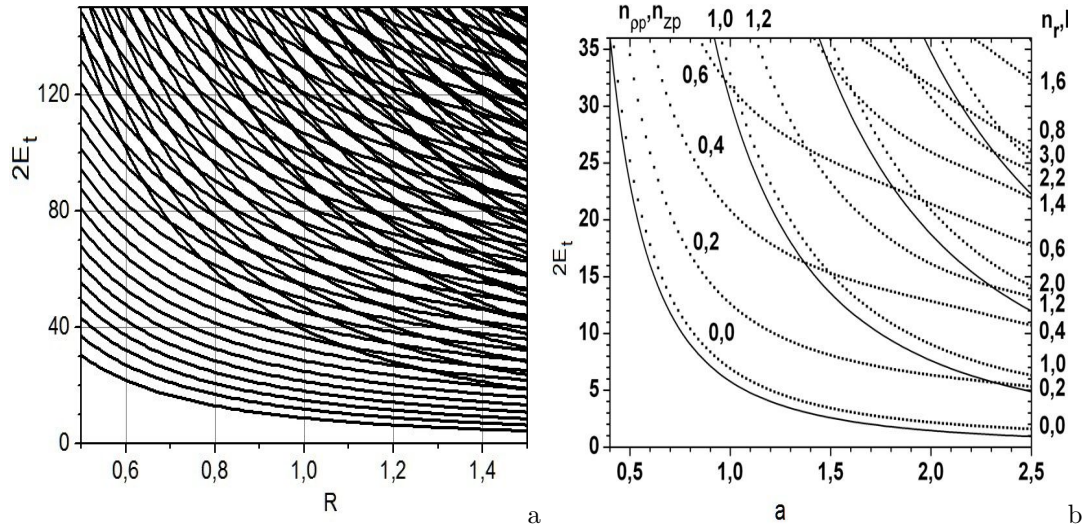

Figure 2. Size quantization energy levels $\mathcal{E}_t = 2E_t = \tilde{E}_i^{SQ}/E_R$ at $m = 0$: a) for prolate CQDs of similar height $H = 10a_B$ versus base radius Ra_B, and b) prolate SQDs with similar major semiaxes $c = 2.5a_B$ versus minor semiaxis aa_B. Here the solid curves are the low adiabatic estimations of eigenvalues $[n_{\rho p}, n_{zp} = 0]$ of the " fast" subsystem.

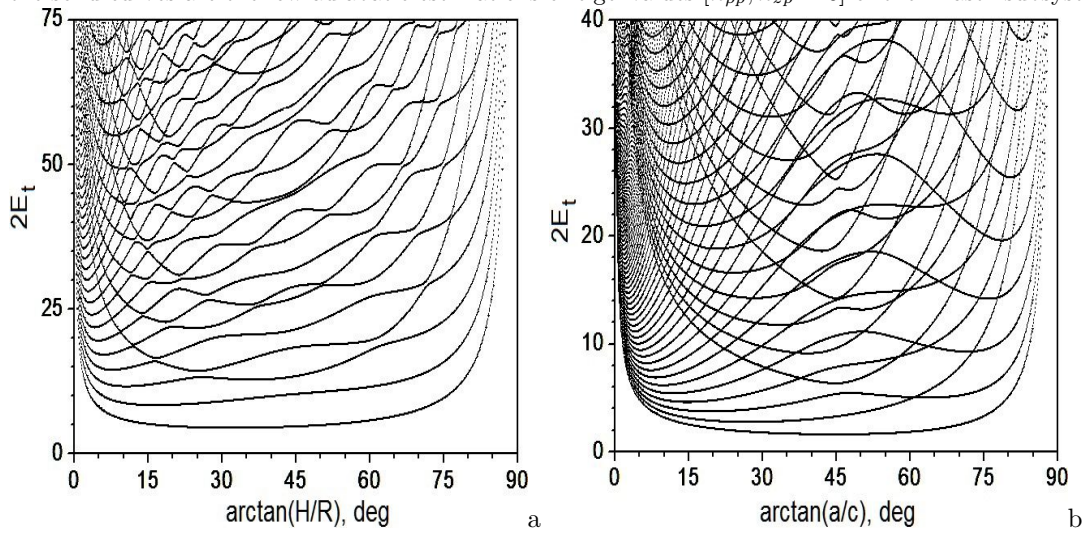

Figure 3. The energy levels $\mathcal{E}_t = 2E_t = \tilde{E}_t^{SQ}/E_R$ at $m = 0$: a) for prolate and oblate CQDs of equal volume $V = \pi R^2 H/3 = (15/2)\pi a_B^3$ at the base of $H = 10$ and $R = 1.5$ versus the stretch angle $\theta_0 = \arctan(H/R)$ at the base of $\theta_0 \approx 8.53^o$, and b) for prolate and oblate SQDs of equal volume $V = 4\pi a^2 c/3 = (125/6)\pi a_B^3$ at the base of $a = c = 2.5$ versus $\theta_0 = \arctan(a/c)$ at the base of $\theta_0 = 45^o$.

Figures 3 a and 3 b for CQD and prolate SDQ show that the faster growth of energy at small apex angles θ_0 is caused by the size quantization in radial variable ρ and angular variable φ. The slower increase of energy at the apex angles approaching the right angle, is caused by the size quantization in longitudinal variable z, i.e., the height. The difference in the rate of energy level variation in the adiabatic domains of variation of geometric parameters is due to the nonuniform scale, since the radius varies as $(\tan\theta_0)^{2/3}$ and the height as $(\cot\theta_0)^{1/3}$. It is also seen that for the angle values beyond the adiabatic domains there are series of quasicrossings and exact crossings of energy levels for CQD and SQD, respectively, and its transformation to the oblate QDs.

5. INTERBAND ABSORPTION

Consider the direct interband absorption in conical quantum dots in the regime of strong size quantization, when the Coulomb interaction between an electron and a hole can be neglected. Furthermore, consider the case of a

Table 2. Comparison of the Coulomb interaction energy $\mathcal{E}_t^{eh}$ and the size quantization energy $\mathcal{E}_t^{SQ}$ in the units of E_R. Here $H = 10a_B$, $m = 0$. The values of $\mathcal{E}^{SQ}_{(tn_pn_{zp}m)}$ (adiabatic calculation) and $\mathcal{E}^{eh}_{(tn_pn_{zp}m)}$ (first-order perturbation theory) adopted from Ref.[4] are labeled by an asterisk.

R (a_B)	$(t, n_\rho, n_z) = (1, 0, 0)$		$(t, n_\rho, n_z) = (18, 1, 0)$		$(t, n_\rho, n_z) = (2, 0, 1)$	
	$\mathcal{E}_t^{SQ}$	$\mathcal{E}_t^{eh}$	$\mathcal{E}_t^{SQ}$	$\mathcal{E}_t^{eh}$	$\mathcal{E}_t^{SQ}$	$\mathcal{E}_t^{eh}$
0.5	30.42114	–2.64009	142.96526	–4.19801	36.95117	–1.88114
0.5	26.624*	–1.121*	141.542*	–1.113*	34.483*	–0.95*
1.0	8.88906	–1.71413	39.22966	–2.27799	11.93808	–1.25028
1.0	8.359*	–0.902*	36.272*	–1.021*	10.287*	–0.608*
1.5	4.49383	–1.33844	18.79476	–1.66173	6.51718	–0.99660
1.5	4.071*	–0.781*	18.085*	–0.762*	5.193*	–0.503*

heavy hole with $m_e^* \ll m_h^*$, where m_e^* and m_h^* are the electron and hole effective mass, respectively. Then the absorption coefficient is given by[9]

$$\tilde{K}(\tilde{\omega}^{ph}) = \sum_{\nu\nu'} \tilde{K}_{\nu\nu'}(\tilde{\omega}^{ph}) = \tilde{K}_0 \sum_{\nu\nu'} \left| \int \tilde{\Psi}^e_\nu \tilde{\Psi}^h_{\nu'} d\vec{r} \right|^2 \delta(\hbar\tilde{\omega}^{ph} - \tilde{E}_g - \tilde{E}^e_\nu - \tilde{E}^h_{\nu'}), \tag{5}$$

where $\tilde{\Psi}^{e(h)}_{\nu(\nu')}$ are envelopes of the electron and hole wave functions, $\nu = [n_{\rho p} n_{zp} m]$ and $\nu' = [n'_{\rho p} n'_{zp} m']$ ($\nu = [n_{zo} n_{\rho o} m]$ and $\nu' = [n'_{zo} n'_{\rho o} m']$) are sets of quantum numbers corresponding to the electron and the heavy hole prolate(oblate) SQD or CQD, respectively, $\tilde{E}_g$ is the band gap of the bulk semiconductor (for GaAs $\tilde{E}_g/E_R = 1.43/(5.27 \cdot 10^{-3})$), $\tilde{\omega}^{ph}$ is the frequency of the incident light, and $\tilde{K}_0$ is proportional to the square of the transition matrix element calculated with Bloch functions.[9] Here the following selection rules for the transitions between the levels with different quantum numbers are valid in the adiabatic classification. In the case of the prolate(oblate) SQD and CQD for the magnetic quantum number the transitions between the levels with $m = -m'$ are allowed. For the prolate(oblate) SQD the transitions between the levels with $n_{\rho p} = n'_{\rho p}$ and $n_{zp} = n'_{zp}$ ($n_{zo} = n'_{zo}$ and $n_{\rho o} = n'_{\rho o}$), respectively, are allowed. For the prolate(oblate)CQD transitions between the levels with $n_{\rho p} = n'_{\rho p}$ ($n_{zp} = n'_{zp}$) are allowed, however there is no selection rule for the axial(radial) quantum numbers n_{zp} ($n_{\rho o}$) and any transitions between different levels are allowed: $n_{zp} \to \forall n'_{zp}$ ($n_{\rho o} \to \forall n_{\rho o}$) respectively, like for prolate (oblate) SQD in uniform electric field[3].

The difference between the energy levels for CQD of the same family is increased with the increase of the axial quantum number. For example, $\Delta\tilde{E}_{10} = 1.12E_R$, when $\tilde{R} = 1.5a_B$ and $\tilde{H} = 10a_B$ ($n_{\rho p} = 0$, $m = 0$), and $\Delta\tilde{E}_{10} = 3.4E_R$, when $\tilde{R} = 1.5a_B$ and $\tilde{H} = 10a_B$ ($n_{\rho p} = 1$, $m = 0$). Note that the transition frequency between these energy levels is $\Delta\tilde{\omega}^{ph}_{10}(n_{\rho p} = 0, m = 0) = 1.43 \cdot 10^{12}\text{sec}^{-1}$ and $\Delta\tilde{\omega}^{ph}_{10}(n_{\rho p} = 1, m = 0) = 4.3 \cdot 10^{12}\text{sec}^{-1}$, which falls into the IR range of spectrum. second In CQD the decrease of the base radius increases the absorption edge energy. It is due to the fact that with the decrease of $\tilde{R}$ the effective width of the bandgap increases due to smaller influence of the CQD walls. The energy levels corresponding to high values of the cone height are located above. Note that the interband transition frequency between the energy levels is $\tilde{\omega}^{ph}_{000} = 5.07 \cdot 10^{-14}\text{sec}^{-1}$ for $\tilde{R} = 0.2a_B$ and $\tilde{H} = 15a_B$, which falls into the visible spectral range.[4]

For the Lifshits-Slezov distribution Fig. 4 displays the total absorption coefficient $\tilde{K}(\tilde{\omega}^{ph})/\tilde{K}_0$ and the partial absorption coefficients $\tilde{K}_{\nu,\nu}(\tilde{\omega}^{ph})/\tilde{K}_0$, that form the corresponding partial sum (5) over a fixed set of quantum numbers ν, ν' at $m = -m' = 0$. In the regime of strong dimensional quantization the frequencies of the interband transitions ($h \to e$) in GaAS between the levels $n_o = n_{zo} + 1 = 1, n_{\rho o} = 0, m = 0$ for oblate SQD or $n_p = n_{\rho o} + 1 = 1, n_{zp} = 0, m = 0$ for prolate SQD at the fixed values $\tilde{a} = 2.5a_e$ and $\tilde{c} = 0.5a_e$ for oblate SQD or $\tilde{a} = 0.5a_e$ and $\tilde{c} = 2.5a_e$ for prolate SQD, are equal to $\Delta\tilde{\omega}^{ph}_{100}/(2\pi) = 16.9\text{THz}$ or $\Delta\tilde{\omega}^{ph}_{100}/(2\pi) = 33.3\text{THz}$, where $\Delta\tilde{\omega}^{ph}_{100}/(2\pi) = (2\pi\hbar)^{-1}(\tilde{W}_{100,100} - \tilde{E}_g)$, $\tilde{W}_{\nu,\nu'} = \tilde{E}_g + \tilde{E}^e_\nu + \tilde{E}^h_{\nu'}$ corresponds to the IR spectral region, taking the band gap value $(2\pi\hbar)^{-1}\tilde{E}_g = 346$ THz into account.[3]

With the decreasing semiaxis the threshold energy increases, because the "effective" band gap width increases, which is a consequence of the dimensional quantization enhancement. Therefore, the above frequency is greater

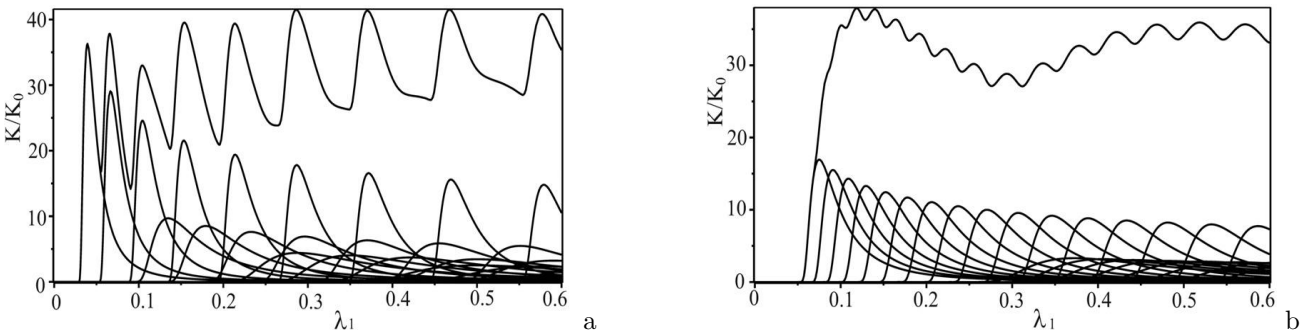

Figure 4. Absorption coefficient K/K_0, Eq. (5), consisting of a sum of the first partial contributions vs the energy $\lambda = \lambda_1 = (\tilde{\omega}^{ph} - \tilde{E}_g)/\tilde{E}_g$ of the optical interband transitions for ensembles of GaAs SQDs ($h \to e$) with the Lifshits-Slezov distribution of the random small semiaxis: a)for an ensemble of oblate SQDs $\bar{c} = 0.5$, $a = 2.5$ and b) prolate SQDs $\bar{a} = 0.5$, $c = 2.5$.

for prolate QD than for oblate QD, because the QD implemented in two directions of the plane (x,y) is effectively larger than that in the direction of the z axis solely at similar values of semiaxes. Higher-accuracy calculations reveal essential difference in the frequency behavior of the AC for interband transitions in the systems of semiconductor oblate or prolate QDs having a distribution of minor semiaxes, which can be used to verify the above models.

6. CONCLUSION

In this paper we demonstrate the efficient methods and software for calculating the electron, hole and exciton states in axially symmetric QDs by the example of conical and spheroidal impenetrable QDs. Our analysis shows that the calculation schemes of FEM of high order implemented on unstructured grids together with complementary KM and AA provide useful numerical and analytical tools for describing the energy spectra and the optical absorption coefficient in an ensemble of non-interacting axially symmetric QDs. Further development and application of such approach and software is associated with the investigation of spectral and optical characteristics of quantum dots with complex geometry.

The work was partially supported by the Russian Foundation for Basic Research (grants Nos. 16-01-00080 and 17-51-44003 Mong_a) and the RUDN University Program 5-100.

REFERENCES

1. Harrison, P.,[Quantum Well, Wires and Dots. Theoretical and Computational Physics of Semiconductor Nanostructures], Wiley, New York (2005).
2. Ramdas Ram-Mohan, L., [Finite Element and Boundary Element Applications in Quantum Mechanics], Oxford Univ. Press, New York (2002).
3. Gusev, A. A., Hai, L. L., Vinitsky, S. I., et al, "Analytical and numerical calculations of spectral and optical characteristics of spheroidal quantum dots," Phys. Atom. Nucl. 76, 1033-1055 (2013).
4. Hayrapetyan, D.B., Chalyan, A.V., Kazaryan, E.M., and Sarkisyan, H.A., "Direct interband light absorption in conical quantum dot" J. Nanomaterials 2015, 915742 (2015)
5. Gusev, A. A., Gerdt, V. P., Chuluunbaatar, O., et al, "Symbolic-numerical algorithms for solving the parametric self-adjoint 2D elliptic boundary-value problem using high-accuracy finite element method," Lecture Notes in Computer Sci. 10490, 151-166 (2017).
6. Gusev, A. A., Gerdt, V. P., Chuluunbaatar, O., et al, "Symbolic-numerical algorithm for generating interpolation multivariate hermite polynomials of high-accuracy finite element method," Lecture Notes in Computer Sci. 10490, 134-150 (2017).
7. Ciarlet, P., [The Finite Element Method for Elliptic Problems], North-Holland Publ. Comp, Amsterdam (1978).
8. Abramowitz, M., and Stegun, I.A., [Handbook of Mathematical Functions], Dover, New York (1965).
9. Anselm, A., [Introduction to Semiconductor Theory], Mir, Moscow (1982), in Russian.